

NASA CONTRACTOR REPORT

NASA CR-129028

(NASA-CR-129028) ATMOSPHERIC EFFECTS ON
REMOTE SENSING OF NON-UNIFORM TEMPERATURE
SOURCES Final Report, Mar. 1973 - Apr.
1974 (South Alabama Univ., Mobile.)
44 p HC \$5.25

N74-25878

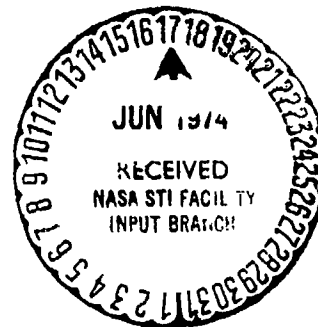
Unclas
39957
CSCL 04A G3/13

ATMOSPHERIC EFFECTS ON REMOTE SENSING OF NON-UNIFORM TEMPERATURE SOURCES

By William A. McNeill and Barry P. Dixon
Department of Mechanical Engineering
Division of Engineering
University of South Alabama
Mobile, Alabama 36688

May 1, 1974

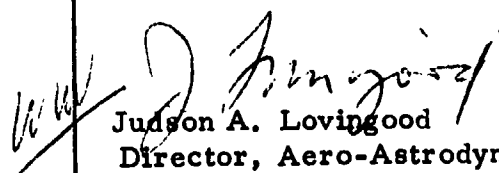
Final Report



Prepared for

NASA-GEORGE C. MARSHALL SPACE FLIGHT CENTER
Marshall Space Flight Center, Alabama 35812

TECHNICAL REPORT STANDARD TITLE PAGE

1. REPORT NO. NASA CR-129028	2. GOVERNMENT ACCESSION NO.	3. RECIPIENT'S CATALOG NO.	
4. TITLE AND SUBTITLE Atmospheric Effects on Remote Sensing of Non-Uniform Temperature Sources		5. REPORT DATE May 1, 1974	
		6. PERFORMING ORGANIZATION CODE	
7. AUTHOR(S) William A. McNeill, Barry P. Dixon		8. PERFORMING ORGANIZATION REPORT #	
9. PERFORMING ORGANIZATION NAME AND ADDRESS Department of Mechanical Engineering Division of Engineering University of South Alabama Mobile, Alabama 36688		10. WORK UNIT NO.	
		11. CONTRACT OR GRANT NO. Contract NAS8-28722	
12. SPONSORING AGENCY NAME AND ADDRESS National Aeronautics and Space Administration Washington, D. C. 20546		13. TYPE OF REPORT & PERIOD COVERED Final Report March 1973 - April 1974	
		14. SPONSORING AGENCY CODE	
15. SUPPLEMENTARY NOTES This work was performed under the direction of the Aerospace Environment Division, Aero-Astro dynamics Laboratory, Science and Engineering Directorate.			
16. ABSTRACT <p>This investigation considers the effects of an absorbing, emitting, and scattering atmosphere upon the remote sensing of surface areas having non-uniform intensity. These atmospheric effects may be significant in determination, by remote sensing, of non-uniform surface temperature distributions, and the results of this investigation are applicable in such cases.</p> <p>Analytical methods and a digital computational program are presented, expressing the results in terms of contrast and contrast transmittance between two adjacent emitting areas having unequal intensities, in the presence of additional "disturbing" emitters. In the computational procedure, emitting areas are replaced by point-source emitters, each assigned an effective intensity based upon the intensity of the area it replaces. Absorbing, emitting, and scattering behavior of the atmosphere may be specified in the computational procedure either by means of analytical atmospheric models or by means of "calibrating" ground level emitters, described in this report.</p>			
17. KEY WORDS Remote Sensing Atmospheric Effects Radiant Energy Absorption Emission Scattering		18. DISTRIBUTION STATEMENT  Judson A. Lovingood Director, Aero-Astro dynamics Lab.	
19. SECURITY CLASSIF. (of this report) UNCLASSIFIED	20. SECURITY CLASSIF. (of this page) UNCLASSIFIED	21. NO. OF PAGES 42	22. PRICE NTIS

PREFACE

A method is presented through which estimates may be made of the effect of an absorbing, emitting, and scattering atmosphere upon remote sensing of surface areas having non-uniform intensity. Results, presented in terms of contrasts and contrast transmittances, may be employed to predict or correct remotely sensed visible or infrared images.

This work was accomplished under the technical monitorship of Mr. Paul Larsen and Mr. S. Clark Brown of the Aerospace Environment Division, Marshall Space Flight Center, Alabama.

PRECEDING PAGE BLANK NOT FILMED

NOMENCLATURE

A - Area
C(0) - Ground level contrast
C(h) - Contrast at altitude h
CT - Contrast Transmittance
e - Hemispherical emissive power
e_p - Black-body hemispherical emissive power
h - Sensor altitude
I - Intensity
I_{eff} - Effective point-source intensity
I₀ - Ground level intensity
R - Distance from sensor line-of-sight ground intercept to effective point source
z - Altitude
β_s, β_a - Scattering and absorption coefficient, respectively
τ_s, τ_a - Optical depth, based on scattering and absorption, respectively
θ - Inclination of sensor line-of-sight with vertical
φ - Rotational angle locating effective point source (Figure 1)

NOMENCLATURE FOR APPENDIX I

a₁, a₂, a₃ - Lower limits on integral
b₁, b₂, b₃ - Upper limits on integral
c₁, c₂, c₃ - Constants in matrix formulation (Equation [5])
f - Function of variables x, y, z
I - Value of integral
I_{n_i} - Trapezoidal approximation of I, using n_i intervals
ñ - Number of intervals in approximate integration
N - n + 1
V - Volume of integration
W_i - ith weight function in approximate integration
x, y, z - Independent variables of integral
α, β, ξ - Values of x, y, z, respectively, at which derivatives are evaluated (Equations [1], [4])

Table of Contents

	<u>Page</u>
Introduction.	1
Contributing Factors in Remote Pattern Sensing	1
Scattering Atmosphere - Results for a Point Source	3
Scattering Atmosphere - Results for Finite Areas	5
Numerical Methods.	7
Absorbing/Emitting Atmosphere.	7
Contrast and Contrast Transmittance	8
Application of Results to Remote Sensing Experiments	9
Computer Program	11
Numerical Example	12
Conclusions.	17
Acknowledgments.	18
Appendix I - Extrapolative Method of Numerical Integration	19
Appendix II - Listing of Computer Program.	25
References	30

List of Figures

Figure 1 - Geometry of Sensor Line-of-Sight for Point Source Emission with Scattering Atmosphere.	31
Figure 2 - Intensity Ratio I/I_0 Versus Distance Ratio R/h and Optical Depth τ_s . Scattering Atmosphere. $\theta = 0^\circ$	32
Figure 3 - Intensity Ratio I/I_0 Versus Distance Ratio R/h and Optical Depth τ_s . Scattering Atmosphere. $\theta = 22\ 1/2^\circ$	33
Figure 4 - Intensity Ratio I/I_0 Versus Distance Ratio R/h and Optical Depth τ_s . Scattering Atmosphere. $\theta = 45^\circ$	34
Figure 5 - Intensity Ratio I/I_0 Versus Distance Ratio R/h and Optical Depth τ_s . Scattering Atmosphere. $\theta = 67\ 1/2^\circ$	35
Figure 6 - Intensity Ratio I/I_0 Versus Distance Ratio R/h and Optical Depth τ . Vertical Line of Sight.	36
Figure 7 - Establishment of Emission Point Sources in an Area of Non-Uniform Intensity.	37
Figure 8 - Input and Output Data for Computer Program Listed In Appendix II	38
Figure 9 - Geometry of Example Illustrating Computation of Contrast Transmittance	39

ATMOSPHERIC EFFECTS ON REMOTE SENSING OF
NON-UNIFORM TEMPERATURE SOURCES
FINAL REPORT

INTRODUCTION

This investigation considers the effects of atmospheric participation upon the remote sensing of the earth's surface when that surface exhibits a ground-level intensity which varies from point to point. This ground level intensity may be produced by emission at the surface, reflection, or both. Since the emitted energy is dependent upon the surface temperature, it is possible to infer the surface temperature by means of remote measurements, when an estimate is made of atmospheric participation and other effects, to be discussed. Of particular interest in this investigation is the effect of "disturbing" emitting areas, not in the sensor line-of-sight, but whose energy is scattered into the sensor line-of-sight, producing an interfering signal at the sensor. It is the purpose of this investigation to provide methods of predicting remotely sensed contrast between two surface areas having unequal intensities, and compare that contrast to the contrast at the ground between the two areas, giving a "contrast transmittance". Knowing the contrast transmittance, it is possible to interpret remotely sensed visible or infrared images with respect to resolution, loss of detail, and other important aspects of pattern recognition. If preliminary atmospheric measurements indicate, for example, that an unacceptable loss of contrast would occur, a sensing run might be delayed pending more favorable conditions.

CONTRIBUTING FACTORS IN REMOTE PATTERN SENSING

Several factors complicate remote pattern recognition. If it is assumed that the upwelling radiant energy is due solely to the surface

temperature, a larger change in energy received by the sensor will occur per degree of change in temperature for a warm surface than for a cool surface. Bastuscheck (Reference 1) has discussed this effect. The radiant energy received from a highly reflecting surface area, however, is not indicative of its temperature. For this reason, it is preferable to think in terms of upwelling intensity or radiancy, with the understanding that this energy may result from emission, reflection, or both. For the remote sensing of surface temperatures, ground-level correlations must be made between surface temperature and total upwelling energy, taking into account specific emissive and reflective properties of the surface. Thus the significant surface characteristic for the purposes of this investigation is taken to be upwelling intensity.

Of great importance is the wavelength or frequency interval in which the sensing takes place. Not only does the rate of upwelling energy from a given surface area vary greatly with wavelength, but scattering, emitting and absorbing effects of the atmosphere, which attenuate the signal from the surface, vary dramatically with wavelength. In addition, the attenuating effects of the atmosphere vary with location and time of year. Anding (Reference 2) and Chang (Reference 3) have performed detailed studies of atmospheric attenuation, and the 4-D atmospheric model of Chang is incorporated into the final results of this investigation.

Also of great importance in this investigation is the geometry of the sensor line-of-sight with respect to the vertical, and with respect to "disturbing" emitters.

SCATTERING ATMOSPHERE. RESULTS FOR A POINT SOURCE

This report is an extension of the investigation of Reference (4). For continuity some of the results of that report will be included here. In the previous report the purely scattering behavior of the atmosphere was studied with respect to a single "disturbing" point source of known intensity I_0 , erg/sec-m²-steradian-m, not lying in the sensor line-of-sight. The sensor is inclined at an angle θ from the vertical and an angle ϕ with respect to a line from the line-of-sight ground intercept to the point source (Figure 1). The point source lies a distance R from the line-of-sight ground intercept. The vertical altitude is h , kilometers, and an average scattering coefficient β_s , 1/kilometer, assumed constant, gives an optical depth, based on vertical elevation, of $\beta_s h$. (Optical depth (dimensionless) based on scattering, τ_s , is defined as $\tau_s \equiv \int_0^h \beta_s dz$. The final program in Appendix II includes the effect of a variable scattering coefficient, as a function of altitude z .) Scattering by the atmosphere is assumed to be isotropic. Except for the point source, the surface is assumed to be black and non-emitting. Letting I denote the intensity at the location and in the direction and sense of the sensor, a solution was found in Reference (4) for I/I_0 as a function of the dimensionless variables θ , ϕ , R/h and $\beta_s h$. The solutions presented in Reference (4), for optical depths to .1 are reproduced in Figures (2) through (5). The program used to compute the data plotted in these figures is included as part of the final program, in Appendix II, in order that additional data of this type may be obtained if needed. Presented in dimensionless form, the results are valid for any values of R , h , and β_s corresponding to the wavelength interval under consideration.

Although the small optical depths appearing in Figures (2) through (5) are representative of the scattering behavior for a large range of cases encountered in practice, it is necessary to extend the previous results to larger optical depths in order to discern more general patterns of the effect of the point source "disturbing" emitter. Accordingly, the data of Figure (2) ($\theta=0$) was extended to larger optical depths and presented in Figure (6). Some interesting results are noted, as follows:

- (1) For small optical depths ($<.1$) the curves are relatively flat, and I/I_0 increases with increasing optical depth.
- (2) With increased optical depth to around 1, the curves show a quicker drop-off with R/h .
- (3) As the optical depth continues to increase beyond 1, however, the maximum value of I/I_0 (at $R/h=0$) begins to decrease with increased optical depth. Finally, as shown in Figure (6), I/I_0 vanishes for very large optical depths as it did for very small optical depths.
- (4) For larger values of R/h , the maximum value of I/I_0 occurs with smaller values of $\beta_s h$.

The value of $\beta_s h$ for which I/I_0 attains its maximum value is of some theoretical interest. No attempt was made in this investigation to precisely determine this value; however, an order-of-magnitude estimate indicated that for this vertical line-of-sight case the maximum would occur for $\beta_s h < 2$. The existence of a value of $\beta_s h$ for which the influence of the "disturbing" point is maximum is expected, and may be illustrated by the following example: Consider as a "sensor" a person standing on earth looking upward, not at the sun, and regard the sun as the "disturbing"

point source. If there were no atmosphere (i.e., very small optical depth) no energy would be scattered into the "sensor" line of sight (i.e., I/I_0 would be zero). Next consider a clear atmosphere. The optical depth is moderate due to scattering, and the "sensor" receives considerable visible radiation (i.e., I/I_0 is greater than zero). Finally, as the sky becomes overcast, making δh larger, a decrease in I/I_0 is noted, indicating that the "peak" value has been passed.

SCATTERING ATMOSPHERE. RESULTS FOR FINITE AREAS

The versatility of application of the results obtained for the point source is evident in the extension of the investigation to consideration of "disturbing" emitting areas of finite extent. Several emitting areas are, for computational purposes, replaced by point sources, each located within the boundary of an original area, and each point source assigned an "effective" intensity I_{eff} , erg/sec-meter²-steradian-meter. The effective intensity assigned to a point source is determined by the requirement that the point source have the same total hemispherical rate of energy emission in the same frequency interval as the original area it replaces. For a diffuse emitter the total hemispherical emissive power

e (energy rate per area per frequency interval, erg/sec-meter²-meter) is related to the intensity by the relation $e = \pi I$ (Reference 5). Thus the total rate of energy emission per frequency interval becomes $eA = \pi IA$, where A is the emitting area. The point source replacement of the finite area is made by assigning I_{eff} the value obtained by normalizing the "effective" emitting area to unity, maintaining the same hemispherical emissive power, i.e., $I_{\text{eff}}(1) = I_0 A$, where I_0 is the intensity corresponding

to area A. This process will be exact as the size of the original emitting area approaches zero (or more precisely as $A/h^2 \rightarrow 0$). In the computational procedure, A approaches zero numerically by an integration technique.

Figure (7) illustrates the method. A given area A is assumed to have non-uniform intensity. A four-division approximate integration of the contribution due to emission from that area is indicated in the figure, in which each area segment ΔA_i is replaced by a point source having an effective intensity $I_{ieff} = I_i \Delta A_i$, located within the boundary of the corresponding area segment. Each point source is then treated by the methods previously developed, noting that the point sources in general differ in their values of R/h and ϕ with reference to the sensor line-of-sight. The extension to a larger number of divisions for areas over which the intensity varies is clear. Numerical examples will be presented in a later section illustrating the methods developed above.

The above discussion considers the influence of emitted energy from points not at the sensor line-of-sight ground intercept. If, as is the usual case, the ground intercept point (i.e., the "target" point) is emitting energy, the sensor will receive energy directly from that point. This signal will be affected by the atmosphere, and will be reduced in intensity by a fraction $e^{-\tau_s/\cos\theta}$, known as the atmospheric "transmittance". In addition, the "target" itself may act in the role of a "disturbance", since some of its energy emitted in a direction not along the line-of-sight may be scattered into the sensor by the atmosphere. This "disturbance" aspect of the "target" may be treated as a special case of a "disturbance" for which $R=0$ in Figure (1).

NUMERICAL METHODS

A discussion of the numerical method employed to solve the integro-differential equations governing the scattering problem was presented in Reference (4). Some results pertaining to the numerical method itself will now be presented. Evaluation of the multiple integrals appearing in the governing equations is quite time-consuming on the digital computer. Consequently, methods were sought which would evaluate fixed-limit multiple integrals while optimizing accuracy and computation time. In the course of the investigation a very useful iterative method of multiple integration was developed and employed to obtain some of the numerical data. This method is presented in Appendix I. After development of the method it was determined that the extreme accuracy it provided was not necessary by comparison with the number of significant figures carried in the remainder of the computational process, and therefore the iterative method does not appear in the final program in Appendix II.

ABSORBING/EMITTING ATMOSPHERE

The investigation has thus far dealt with a scattering atmosphere, that is, one which neither absorbs nor emits radiant energy. Absorption and emission by the atmosphere are of great importance in remote sensing, and the governing equations for a non-scattering atmosphere are considerably simpler than those for scattering atmospheres. In such an atmosphere, only those processes of emission and absorption which occur on the sensor line-of-sight need be considered, and there is no contribution to energy received by the sensor from any "disturbing" emitter not on the line-of-sight.

For the non-scattering atmosphere, Reference (5) or (6) readily gives the equation for the intensity received at the sensor location, in the direction and sense of the line-of-sight as follows:

$$I = I_0 e^{-\tau_a/\cos\theta} + \frac{1}{4\pi} \int_0^{\tau_a} e_b e^{-(\tau_a-t)/\cos\theta} \frac{dt}{\cos\theta}, \quad [1]$$

where I_0 now represents the intensity at the ground level line-of-sight intercept, e_b denotes the black-body hemispherical emissive power, and τ_a represents the optical depth based on absorption, i.e., $\tau_a = \int_0^h \beta_a dz$. The symbol β_a denotes the absorption coefficient, which may in general be a function of altitude z . The symbols θ , z , and h have the same interpretation as in Figure (1), and t denotes a dummy variable of integration. The hemispherical black-body emissive power e_b is a function of the wavelength at which the intensity is computed and the absolute temperature of the atmosphere. Reference (7) may be consulted for a theoretical discussion of this function. In order to obtain the value of the intensity I received by the sensor it is necessary to perform a numerical integration as indicated in the above equation, given I_0 , θ , h , and the variation of the absorption coefficient and temperature as functions of altitude. This numerical integration is performed as part of the final program in Appendix II.

CONTRAST AND CONTRAST TRANSMITTANCE

Two of the most important aspects of remote sensing of non-uniform targets are contrast and contrast transmittance. Given a "target" and an

adjacent "background", denoted by t and b , respectively, the contrast at ground level, based on intensity at a specified wavelength, is defined to be

$$C(0) = I_t(0)/I_b(0) , \quad [2]$$

where the (0) denotes intensities at ground level, and the "target" may be assumed, without loss of generality, to have the higher intensity. Let $I_t(h)$ and $I_b(h)$ denote intensity at the sensor, at altitude h , when the line-of-sight passes at ground level through points t and b , respectively. The contrast at altitude h is given by $C(h) = I_t(h)/I_b(h)$. In general $C(h)$ will be smaller than $C(0)$ due to atmospheric participation, including the effects of "disturbing" emitters on the surface. The reduction in contrast is specified by the contrast transmittance CT , defined as $C(h)/C(0)$, and it is the contrast transmittance which measures the degree of pattern recognition possible. Miller, et al, (Reference 8) have presented some typical measured contrast transmittance values and discussed additional aspects of multispectral sensors for ERTS A & B.

APPLICATION OF RESULTS TO REMOTE SENSING EXPERIMENTS

A review of ongoing and planned ERTS and SKYLAB capabilities and programs (References 8, 9, and others) was made, with respect to potential input from the results of this investigation. A number of conclusions and recommendations result from this review. Loss of contrast of a ground signal may result from scattering, absorption/emission by the atmosphere, or a combination of these effects. In some regions of the wavelength spectrum one may be fairly certain that one effect or the other dominates the atmospheric attenuation (for example, attenuation in the visible

range is almost entirely due to scattering). In general, however, it cannot be expected that the attenuation will be positively identifiable as to mode. In this regard it may be noted that the development in this investigation has assumed that the atmosphere is either purely scattering or is totally non-scattering. This distinct separation was made to streamline the application of the results, in view of the practical inability to identify in general the mode of attenuation. Several important parameters can, however, be accurately measured or predicted. The sophisticated 4-D atmospheric model of Chang (Reference 3) provides reliable temperature and other property profiles, as well as total transmissivity. In addition, total transmissivity is conceptually simple to measure experimentally (although it is in general not possible to identify whether the attenuation is due to absorption, scattering, or both). An experimental procedure for use in conjunction with a contrast computational procedure might proceed as follows: Establish two "calibrating" emitters on the ground, emitting radiant energy of different intensities in the same frequency range, and positioned in the proximity of the areas between which it is desired to determine contrast by remote sensing. These adjacent ground emitters would be remotely sensed, and the transmissivity thereby determined, as the ratio of the difference between the remotely sensed intensity when viewing, in turn, the two calibrating emitters to the difference between the known ground values of intensity of the emitters. This would be valid for any combination of scattering/absorbing/emitting attenuation, since the atmospheric emission would subtract out due to the taking of a difference ratio. Knowing the

total transmissivity, the limits on the contrast between the two emitting areas in question may be determined by (a) assuming the atmosphere to be purely scattering and then (b) assuming the atmosphere to be non-scattering. In both cases (a) and (b) the measured or estimated transmissivity is used. Then the contrast and contrast transmittance for a partially scattering atmosphere may be shown to lie between the two limits found in (a) and (b). If the predicted contrast transmittance range is unacceptably low, considering the known or estimated intensities of "target", "background", and any "disturbing" emitters which may be present, the collection of extensive data could be rescheduled.

COMPUTER PROGRAM

The digital computer program, listed in Appendix II, accepts as input data the geometry of the sensor line-of-sight with respect to one or more "disturbing" emitting areas whose "effective" point source intensities are also included as inputs. The "target" intensity is also read in, as is the sensor altitude, and the temperature profile computed by the 4-D model of Reference 3. In addition, the program will receive as an input scattering and absorption coefficients as functions of altitude. The program computes the "band" in which the intensity at the sensor location may be found, by assuming the atmosphere to be, respectively, purely scattering and non-scattering. The scattering coefficient is not necessarily constant with altitude as was the case with the preliminary results shown in Figures (2) through (5). Nor is the absorption coefficient necessarily constant with altitude.

If, as discussed in the preceding section, scattering and absorption coefficients are not specified as functions of altitude, but, instead, the total transmissivity is known, an average value of the scattering or

absorption coefficient may be read into the computer program, the value being determined from the known transmissivity. Example calculations in the following section illustrate the computational procedures.

The diagram in Figure 8 summarizes the inputs and outputs of the computer program.

NUMERICAL EXAMPLE

The following example illustrates the use of the results previously obtained, to estimate the effect of atmospheric participation upon contrast and contrast transmittance of upwelling radiant energy, in which the surface distribution of intensity is non-uniform. Figure (9) illustrates a typical situation of this type. It is desired to compute the contrast between emitting area ΔA_1 (the "target") and area ΔA_2 (the "background"), in the presence of a participating atmosphere and a third "disturbing" emitter ΔA_3 . Contrast is to be computed between two adjacent points of areas ΔA_1 and ΔA_2 at the position shown as the sensor line-of-sight ground intercept. For simplicity of calculation each emitting area is replaced by a single point source (rather than a number of point sources as in Figure 7) having an "effective" intensity based on the intensity of the area and the size of the area. Three wavelengths are selected for computation, one in the visible, and the other two in well-known atmospheric "windows". For purposes of comparison among the three wavelengths, the respective intensities of the areas are taken to be the same at all wavelengths considered. This, of course, would not be the case if upwelling radiation were due solely to the area's temperature; but, as discussed earlier, for reflecting areas the upwelling radiation is not necessarily an indication of the surface temperature. The

following table gives values used for all three wavelengths:

<u>i</u>	<u>$\Delta A_i, m^2$</u>	<u>$I_{i0}, \text{erg/sec-m}^2\text{-sr-m}$</u>	<u>I_{ieff}</u>	<u>Average Distance From L.O.S. ground intercept, m.</u>
1 "target"	2	6×10^{14}	12×10^{14}	1
2 "background"	1	4×10^{14}	4×10^{14}	.5
3 "disturbance"	5	6×10^{14}	30×10^{14}	5

(1) $\lambda = .5\mu$

The total atmospheric transmittance at this wavelength may be estimated (Reference 10) to be 0.6. Assuming this to be the only information available regarding atmospheric attenuation (i.e., assuming a detailed correlation between altitude and scattering coefficient is not available for input to the computer program), an average scattering coefficient $\beta_s = .0144$ is read into the program. This value of β_s is chosen to provide an overall transmittance equal to 0.6, since

$$\text{Transmittance} = e^{-\tau_s / \cos \theta} = e^{-\beta_s h / \cos \theta} = e^{-.0144 \times 25 / \cos 45^\circ} = 0.6$$

It is first assumed that the atmospheric attenuation is due solely to scattering. When viewing the target, the magnitude of intensity at the sensor location is due to two contributing sources: First, the intensity at the sensor is equal to that at the target multiplied by the transmittance factor of 0.6, which represents the effect of energy scattered from the sensor line-of-sight by the atmosphere. Second, some energy is scattered into the sensor line-of-sight because of the "disturbing" emitting areas, represented by effective point-source emitters. There are three such "disturbing" emitters, counting the "target", ΔA_1 , "background", ΔA_2 , and the "disturbing" emitter ΔA_3 . Since R/h is very small for all three

effective point sources, the computer program (Appendix II) gives $I/I_0 \approx .0316$ for each effective point source. (It may be noted that this result cannot be obtained from Figure 4 because the optical depth of .36 is not within the range of the data presented in that figure).

Letting $I|_{\text{target}}$ denote the intensity corresponding to the sensor location and orientation when viewing the target, the above-mentioned effects are combined as follows:

$$\begin{aligned} I|_{\text{target}} &= I_{10} e^{-\tau_s/\cos\theta} + (I/I_0) [I_{1\text{eff}} + I_{2\text{eff}} + I_{3\text{eff}}] \quad [3] \\ &= 6 \times 10^{14} e^{-.0144 \times 25/.7071} + .0316 [12 + 4 + 30] 10^{14} \\ &= 6 \times 10^{14} \times .6 + 1.4536 \times 10^{14} \\ &= 5.0536 \times 10^{14} \text{ erg/sec-m}^2\text{-sr-m} \end{aligned}$$

When viewing the adjacent background, the energy received due to "disturbing" emitters is unchanged, but the direct radiation is now received from area ΔA_2 . Thus the intensity at the sensor, when viewing the background, is

$$\begin{aligned} I|_{\text{back}} &= I_{20} e^{-\tau_s/\cos\theta} + (I/I_0) [I_{1\text{eff}} + I_{2\text{eff}} + I_{3\text{eff}}] \quad [4] \\ &= 4 \times 10^{14} \times .6 + 1.4536 \times 10^{14} \\ &= 3.8536 \times 10^{14} \text{ erg/sec-m}^2\text{-sr-m} \end{aligned}$$

The ground contrast is

$$C(0) = I_t(0)/I_b(0) = I_{10}/I_{20} = (6 \times 10^{14})/(4 \times 10^{14}) = 1.5$$

The contrast at the sensor altitude of 25 kilometers is

$$C(h) = I_t(h)/I_b(h) = (5.0536 \times 10^{14})/(3.8536 \times 10^{14}) = 1.3114$$

The contrast transmittance is

$$CT = C(h)/C(0) = 1.3114/1.5 = 87.4\%$$

If the atmosphere is next assumed to have a transmittance of 0.6, but be non-scattering, the computer program evaluates intensities, contrasts, and contrast transmittances according to equation [1]. The results of this computation reveal that the contrast is essentially unchanged, indicating that the atmosphere does not emit appreciably at this wavelength. Thus the contrast transmittance for a non-scattering atmosphere is approximately 100%.

The results are summarized as follows: at a wavelength of 0.5μ , if the total atmospheric transmittance is estimated (or measured using calibrating emitters) to be 0.6, then the contrast transmittance for the above-described intensities, areas, etc. lies in the "band", $87.4\% \leq CT \leq 100\%$.

() $\lambda = 4\mu$

Chang (Reference 3) gives an atmospheric transmittance of .86981 for this wavelength for Region 6 (January) for a cloudless, non-scattering atmosphere. For the purpose of illustrating the computation of the contrast transmittance "band", however, the atmospheric transmittance will be assumed to be .86981 for a purely scattering atmosphere as well as for a non-scattering atmosphere. If it is first assumed that the atmosphere is purely scattering, an average $\beta_s = .00394$ is read into the program to produce the desired atmospheric transmittance of .86981, as previously described. The program gives $I/I_0 = .0109$ for the three "disturbing" effective point sources. Using equations [3] and [4], the intensities at the sensor when viewing, respectively, the target and the background are computed to be

$$\begin{aligned} I|_{\text{target}} &= 6 \times 10^{14} \times .86981 + .0109 [12 + 4 + 30] \times 10^{14} \\ &= 5.7214 \times 10^{14} \text{ erg/sec-m}^2\text{-sr-m,} \end{aligned}$$

$$\begin{aligned} I|_{\text{back}} &= 4 \times 10^{14} \times .86981 + .0109 [12 + 4 + 30] \times 10^{14} \\ &= 3.9814 \times 10^{14} \text{ erg/sec-m}^2\text{-sr-m} . \end{aligned}$$

The ground contrast remains at the value 1.5 for this example. The contrast at the sensor altitude of 25 kilometers is

$$C(h) = I_t(h)/I_b(h) = (5.7214 \times 10^{14}) / (3.9814 \times 10^{14}) = 1.437$$

The contrast transmittance is

$$CT = C(h)/C(0) = 1.437/1.5 = 95.8\%$$

If, next, the atmospheric transmittance of .86981 is assumed to be measured in a non-scattering atmosphere, the computer program employs equation [1] to evaluate the intensities at the sensor location. The following results are obtained:

$$I \Big|_{\text{target}} = 6 \times 10^{14} \times .86981 + .49604 \times 10^{11}$$

$$I \Big|_{\text{back}} = 4 \times 10^{14} \times .86981 + .49604 \times 10^{11}$$

As in the previous case, it is clear that the atmospheric emission (represented by the second term in the above equations) does not greatly affect the signal, so that the contrast transmittance is 100% for this case. The contrast transmittance "band" is thus $95.8\% \leq CT \leq 100\%$.

(3) $\lambda = 10\mu$

Reference 3 gives a transmissivity of .68 for this wavelength for Region 5 (January) for a cloudless, non-scattering atmosphere. As in the previous example, the transmissivity of .68 will be assumed to describe both modes of attenuation, in order to illustrate the computation of a contrast transmittance "band". As before, assuming a purely scattering atmosphere, $C(h) = 1.347$, and $CT = 89.8\%$. For a non-scattering atmosphere, $C(h) = 1.487$, $CT = 99.2$, therefore $89.8\% \leq CT \leq 99.2$.

CONCLUSIONS

The scattering, emitting, and absorbing behavior of the atmosphere is complex, and few generalizations are possible within the visible or infrared spectral regions. Much effort has been devoted to development of atmospheric models to describe this behavior. In this connection, Reference 3, for example, has already been mentioned. The work of Threlkeld and Jordan (Reference 16) discusses in detail atmospheric transmissivity on clear days. Threlkeld and Jordan's results indicate that water vapor and dust scattering are significant well into the infrared region. If detailed atmospheric models are available, they may be incorporated into the program in Appendix II of this report. In many cases, however, local effects (for example, the discharge from a smokestack, clouds, or unusual gas concentrations), may require the use of calibrating emitters, as discussed in a previous section of this report.

Regarding the selection of wavelength bands to employ for remote sensing, again no firm generalizations can be made. Two aspects should be considered, however. First, it is of course desirable to sense in a "window", where transmissivity is high. Such windows are well-known for standard atmospheres. In addition, it is necessary to consider that the emissivity of the atmosphere varies with wavelength, and thus will produce greater interference with the desired signal at some wavelengths than at others. As a rough estimate of the wavelength variation of the atmospheric emissivity, it is useful to compute the wavelength at which the black-body emissive power is greatest, corresponding to an average atmospheric temperature. It may be shown (Reference 5) that $\lambda T = 5216$ gives the wavelength λ , microns, at which a black body having temperature T , °R, has the greatest emissive power.

ACKNOWLEDGMENTS

The authors wish to acknowledge the generous support and assistance of NASA Contracting Officer Representatives, Mr. Paul Larsen and Mr. Clark Brown, throughout the course of this investigation. The excellent technical typing and other clerical work of Miss Susan Sharp is also gratefully acknowledged.

APPENDIX I
EXTRAPOLATIVE METHOD OF
NUMERICAL INTEGRATION

EXTRAPOLATION METHOD FOR MULTIDIMENSIONAL QUADRATURE

A matrix formulation of an extrapolation method for the evaluation of multiple integrals, applicable to any order integral, is shown to be concise and easily programmed. Moreover, it is demonstrated to be efficient from the standpoint of accuracy versus number of operations performed. The method is limited in this investigation to the evaluation of triple integrals with fixed limits, although it may easily be adapted to integrals of higher or lower order. The trapezoidal rule is employed as the fundamental quadrature, although the general multidimensional method can be easily developed using a Simpson's or other rule. Additional examples and analysis of extrapolative methods of this type may be found in references (11) through (15).

Using the triple integral as the basis for the development of the extrapolation method, we assume that a numerical approximation is desired for

$$I \equiv \int_{a_3}^{b_3} \int_{a_2}^{b_2} \int_{a_1}^{b_1} f(x,y,z) dx dy dz,$$

where $f(x,y,z)$ is a continuous function of the variables x , y and z in a volume V , and where the numbers a_1 , a_2 , a_3 , b_1 , b_2 , b_3 , are lower and upper limits, respectively, on x , y , and z in V .

Using the trapezoidal rule, the approximation to the single integral is written as follows:

$$I_1(y,z) \equiv \int_{a_1}^{b_1} f(x,y,z)dx = \sum_{i=1}^N w_i f(x_i,y,z) - \frac{(b_1-a_1)^3}{12 n^2} \left. \frac{\partial^2 f}{\partial x^2} \right|_{\xi,y,z}, a_1 < \xi < b_1, [1]$$

where w_i are the trapezoidal weight functions, n is the number of intervals, and $N \equiv n + 1$. In this equation and the equations to follow, existence of derivatives to the required order in V is assumed. Formally applying this trapezoidal rule to a double integral, it follows that an approximation to the double integral may be written as follows:

$$I_2(z) \equiv \int_{a_2}^{b_2} \int_{a_1}^{b_1} f(x,y,z)dx dy = \sum_{i=1}^N w_i \int_{a_2}^{b_2} f(x_i,y,z)dy - \frac{(b_1-a_1)^3}{12 n^2} \left. \frac{\partial^2 f}{\partial x^2} \right|_{\xi,y,z} dy \quad [2]$$

Similarly, formal application of the rule to a triple integral yields

$$I \equiv \int_{a_3}^{b_3} \int_{a_2}^{b_2} \int_{a_1}^{b_1} f(x,y,z)dx dy dz = \sum_{i=1}^N w_i \int_{a_3}^{b_3} \int_{a_2}^{b_2} f(x_i,y,z)dy dz - \frac{(b_1-a_1)^3}{12 n^2} \int_{a_3}^{b_3} \int_{a_2}^{b_2} \left. \frac{\partial^2 f}{\partial x^2} \right|_{\xi,y,z} dy dz \quad [3]$$

Next, substitutions of the single integral expression are made from equation (1) into equation (2), and expressions for the double integrals appearing in equation (3) are replaced by using equation (2). After some manipulation of the expression resulting from this multiple substitution, the following relation is obtained:

$$I = \int_{a_3}^{b_3} \int_{a_2}^{b_2} \int_{a_1}^{b_1} f(x,y,z)dx dy dz = \sum_{i=1}^N \sum_{j=1}^N \sum_{k=1}^N w_i w_j w_k f(x_i, y_j, z_k) - \frac{(b_3-a_3)^3}{12 n^2} \int_{a_2}^{b_2} \int_{a_1}^{b_1} \left. \frac{\partial^2 f}{\partial z^2} \right|_{x,y,\xi} dx dy$$

$$- \frac{(b_3 - a_3)^3 (b_1 - a_1)^3}{(12)^2 n^4} \int_{a_2}^{b_2} \frac{\partial^2}{\partial x^2} \frac{\partial^2}{\partial z^2} f \Big|_{\xi, y, \beta} dy - \frac{(b_3 - a_3)^3 (b_2 - b_2)^3}{(12)^2 n^4} \int_{a_1}^{b_1} \frac{\partial^2}{\partial y^2} \frac{\partial^2}{\partial z^2} f \Big|_{x, \alpha, \beta} dx$$

$$- \frac{(b_3 - a_3)^3 (b_2 - a_2)^3 (b_1 - a_1)^3}{(12)^3 n^6} \frac{\partial^2}{\partial x^2} \frac{\partial^2}{\partial y^2} \frac{\partial^2}{\partial z^2} f \Big|_{\xi, \alpha, \beta} - \frac{(b_2 - a_2)^3}{12 n^2} \int_{a_3}^{b_3} \int_{a_1}^{b_1} \frac{\partial^2 f}{\partial y^2} \Big|_{x, \alpha, z} dx dz$$

$$- \frac{(b_2 - a_2)^3 (b_1 - a_1)^3}{(12)^2 n^4} \int_{a_3}^{b_3} \frac{\partial^2}{\partial x^2} \frac{\partial^2}{\partial y^2} f \Big|_{\xi, \alpha, z} dz - \frac{(b_1 - a_1)^3}{12 n^2} \int_{a_3}^{b_3} \int_{a_2}^{b_2} \frac{\partial^2 f}{\partial x^2} \Big|_{\xi, y, z} dy dz, \quad \begin{matrix} a_2 < \alpha < b_2 \\ a_3 < \beta < b_3 \end{matrix} \quad [4]$$

The first term on the right of equation (4) represents a trapezoidal rule quadrature of the triple integral, where the number of intervals n is the same for the three axes. To derive an extrapolation formula, it is assumed that four separate quadratures are performed, using four different number of intervals n , viz., n_1, n_2, n_3, n_4 . The symbol I_{n_i} will denote the standard trapezoidal approximation for the i th quadrature, using $n = n_i$ intervals. It is next assumed that the terms multiplying $\frac{1}{n^2}$, $\frac{1}{n^4}$ and $\frac{1}{n^6}$ in equation (4) do not change as n is varied through n_1, n_2 , etc. With this assumption, the four different quadratures may be written as follows:

$$\begin{aligned}
I + \frac{C_1}{n_1^2} + \frac{C_2}{n_1^4} + \frac{C_3}{n_1^6} &= I_{n_1} \\
I + \frac{C_1}{n_2^2} + \frac{C_2}{n_2^4} + \frac{C_3}{n_2^6} &= I_{n_2} \\
I + \frac{C_1}{n_3^2} + \frac{C_2}{n_3^4} + \frac{C_3}{n_3^6} &= I_{n_3} \\
I + \frac{C_1}{n_4^2} + \frac{C_2}{n_4^4} + \frac{C_3}{n_4^6} &= I_{n_4}
\end{aligned}
\tag{5}$$

where C_1, C_2, C_3 denote constants.

These equations may be written in matrix form as follows:

$$\begin{vmatrix} 1 & \frac{1}{n_1^2} & \frac{1}{n_1^4} & \frac{1}{n_1^6} \\ 1 & \frac{1}{n_2^2} & \frac{1}{n_2^4} & \frac{1}{n_2^6} \\ 1 & \frac{1}{n_3^2} & \frac{1}{n_3^4} & \frac{1}{n_3^6} \\ 1 & \frac{1}{n_4^2} & \frac{1}{n_4^4} & \frac{1}{n_4^6} \end{vmatrix} \begin{Bmatrix} I \\ C_1 \\ C_2 \\ C_3 \end{Bmatrix} = \begin{Bmatrix} I_{n_1} \\ I_{n_2} \\ I_{n_3} \\ I_{n_4} \end{Bmatrix}
\tag{6}$$

Solution of these linear equations will yield I , within the limits of the validity of assuming that C_1, C_2 and C_3 remain constant as n is varied. It is observed that the relevant equations for a single and double-integral extrapolation formula may also be obtained from equation (6).

For example, equation (6) produces the single-integral extrapolation formula if C_2 and C_3 are replaced by zeros. Thus if I is interpreted to be the extrapolated approximation of a single integral, its value is obtained from the solution of

$$\begin{vmatrix} 1 & \frac{1}{n_1^2} \\ 1 & \frac{1}{n_2^2} \end{vmatrix} \begin{Bmatrix} I \\ C_1 \end{Bmatrix} = \begin{Bmatrix} I_{n_1} \\ I_{n_2} \end{Bmatrix},$$

a redundant set of equations involving I_{n_3} and I_{n_4} being disregarded. This is recognized as the Romberg extrapolation formula. The extension of the method to higher-dimensional integrals is also evident from the form of equation (6), in which the extrapolation formula for an m th dimensional integral is obtained by replacing $C_{m+1}, C_{m+2} \dots$ by zeros.

Numerical results of this method applied to a triple integral will now be presented. It may first be noted that, except for round-off error, this extrapolation method is exact for monomials of the form $x^a y^b z^c$ where a, b , and c are ≤ 2 , regardless of the choice of n_1, n_2, n_3, n_4 . The method was employed to approximate the integral

$$\int_0^2 \int_0^2 \int_0^2 e^{x+y+z} dx dy dz$$

which has the exact value 260.802. (This value and the following data are rounded off in the 6th significant figure). The following table presents the results of the computation:

<u>n</u>	<u>Trapezoidal Quadrature</u>	<u>Extrapolated Value (n_1, n_2, n_3, n_4)</u>
4	277.373	260.802 (4, 6, 8, 10)
8	264.894	260.802 (12, 16, 20, 24)
10	263.416	
12	262.616	
16	261.821	
20	261.454	
24	261.255	

It is clear that in this case the extrapolation method is desirable. The accuracy of the standard trapezoidal quadrature degenerated due to round-off error, as n was increased, before the accuracy of the extrapolation method was approached.

APPENDIX II
LISTING OF COMPUTER PROGRAM

```

      DIMENSION W(35),Q(8,26),TA(27),TS(27),Z(27)
      C A=CCS(THETA). F=ALTITUDE,KM.
      C XIT=TARGET INTENSITY AT GROUND, ERG/SEC*M**2*SR*M
      C XIB=BACKGROUND INTENSITY AT GROUND, ERG/SEC*M**2*SR*M
      C NS=NUMBER OF DISTURBING EMITTERS
      C B=ANGLE PHI LOCATING IREPT' TH DISTURBING EMITTER
      C RD=DISTANCE OF IREPT' TH DISTURBING EMITTER FROM TARGET
      C XIDIS=EFFECTIVE INTENSITY OF IREPT' TH DISTURBING EMITTERS.
      XINT=0.0
      CALL FOURD(Q)
      N=26
      READ(1,1)A,H,XIT,XIB,NS
      1 FORMAT(2F10.6,2E15.6,12)
      CALL OPDEP(H,N,CA,CS,Q,TA,TS,Z)
      DO 8 I=2,N
      J=I-1
      FCN=ED(Q,J)*EXP(-(CA-TA(J))/A)/A
      XINT=XINT+FCN*(TA(I)-TA(J))
      8 CONTINUE
      DINT=XINT/3.14159
      XIABST=XIT/EXP(CA/A)+DINT
      XIABSB=XIB/EXP(CA/A)+DINT
      DELTA=0.01
      PI=3.14159
      RTA=SQRT(1.-A**2.0)
      DO 99 IREPT=1,NS
      SCAT=0.0
      E=0.0001
      READ(1,35)R,RD,XIDIS
      35 FORMAT(2F10.6,E15.6)
      D=RD/H
      XXX=0.0
      XM=N-1
      DPHI=2.*3.14159/XM
      DXMU=(1.-DELTA)/XM
      DO 100 IE=2,N,2
      JE=IE-1
      XINT=0.0
      CON1=E/A**2.0+D**2.0/E-2.0*D*RTA*CCS(B)/A
      CON2=2.0*E
      CON3=2.0*E*RTA
      CTE=TS(JE)
      K=1
      XMU=DELTA
      6 PHI=0.0
      RTXMU=SQRT(1.-XMU**2.0)
      VAR3=F/(XMU**2.0)
      VAR6=2.0*D*RTXMU
      VAR7=CON3*RTXMU
      JJ=1
      4 VAR1=VAR6*CCS(PHI)/XMU
      VAR4=VAR7*CCS(B-PHI)/(A*XMU)
      VAR5=CON2-VAR4
      I=2
      2 J=I-1
      VAR2=1.-Z(J)/(H*E)
      IF(CTE-TS(J))50,50,52
      50 VAR1=-VAR6*CCS(PHI)/XMU
      VAR5=CON2+VAR4
      52 CONTINUE
      TERM2=E*(CON1-VAR2*(VAR1-VAR3+VAR2+VAR5))

```



```

R=TS(J)*H*SQR(TERM2)/Z(J)
XAB=ARS*(CTE-TS(J))
TLST=R+XAB/XMU
IF(TLST.GT.15.0)GO TO 75
FCN=1.0/(EXP(R+XAB/XMU)*XMU)
M=I+1
IF(I.EQ.N)M=N
XINT=XINT+DXMU*DPHI*(TS(M)-TS(J))*FCN
75 CONTINUE
I=I+2
IF(I-N)2,2,3
3 JJ=JJ+1
PHI=PHI+DPHI
IF(JJ-N)4,4,5
5 K=K+1
XMU=XMU+DXMU
IF(K-N)6,6,7
7 CONTINUE
XIEX=XINT
TERM1=((RTA*COS(B)/A-D/E)*(RTA*COS(B)/A-D/E)+(RTA*SIN(B)/A)**2+1
1.0)**0.5
G=1.0/(EXP(CTE*TERM1))+XIEX/(4.0*PI)
ARG=G/(A*EXP((CS-CTE)/A)**4.*PI)
IT=IE+1
IF(IE.EQ.N)IT=IE
XXX=XXX+ARG*(TS(IT)-TS(JE))
IF(JE-I)55,55,56
55 F=E+.08323333
GO TO 57
56 E=E+.08333333
57 CONTINUE
100 CONTINUE
SCAT=SCAT+XXX*XICIS
99 CONTINUE
XISCAT=XIT/EXP(CS/A)+SCAT
XISCAB=XIB/EXP(CS/A)+SCAT
GCON=XIT/XIB
HCONS=XISCAT/XISCAB
HCUNA=XIABST/XIABSB
CTRANS=HCONS/GCON
CTRANA=HCUNA/GCON
401 FORMAT(60X,'INTENSITY',/)
402 FORMAT(8X,'NON SCATTERING ATMOSPHERE',T85,'SCATTERING ATMOSPHERE',
1//)
403 FORMAT(T13,'TARGET',T43,'BACKGROUND',T85,'TARGET',T99,'BACKGROUND'
1//)
404 FORMAT(61X,'CONTRAST',/)
405 FORMAT(54X,'CONTRAST TRANSMITTANCE',/)
WRITE(3,401)
WRITE(3,402)
WRITE(3,403)
WRITE(3,406)XIABST,XIABSB,XISCAT,XISCAB
WRITE(3,404)
WRITE(3,402)
WRITE(3,407)HCUNA,HCONS
WRITE(3,405)
WRITE(3,402)
WRITE(3,407)CTRANA,CTRANS
406 FORMAT(T9,E15.6,T41,E15.6,T81,E15.6,T97,E15.6,/)
407 FORMAT(T25,E15.6,T89,E15.6//)
CALL EXIT
END

```

```

SUBROUTINE OPDEP(H,N,CA,CS,D,TA,TS,7)
DIMENSION D(8,26),TA(27),TS(27),Z(27)
DZ=H/(N-1)
Z(1)=0.0
TA(1)=0.0
TS(1)=0.0
DO 99 I=2,N
J=I-1
Z(I)=Z(J)+DZ
TA(I)=TA(J)+BETAA(J,D)*DZ
99 TS(I)=TS(J)+BETAS(J,D)*DZ
Z(1)=0.00001
TS(1)=0.00001
CA=TA(26)
CS=TS(26)
RETURN
END

```

```

FUNCTION ER(D,I)
DIMENSION D(8,26)
C XL=WAVELENGTH, METERS
JK=D(3,I)
XL=4.0 E-6
I=6.625 E-27
C=2.998 E 8
B=1.38 E-16
ER=(2.0*3.14159*H*C**2.0)/(XL**5.C*(EXP((H*C)/(XL*B*TK
1)))-1.0))
RETURN
END

```

```

FUNCTION BETAA(I,D)
DIMENSION D(8,26)
C BETAA=ABSORPTION COEFFICIENT, 1/KM
BETAA=0.00324
RETURN
END

```

```

FUNCTION BETAS(I,D)
DIMENSION D(8,26)
C BETAS=SCATTERING COEFFICIENT, 1/KM
BETAS=0.004
RETURN
END

```

```

      SUBROUTINE FOURD(D)
C     COMPUTE- CURVES OF ATMOSPHERE PROPERTIES
      DIMENSION GRT(7),D(8,26),YY(11),ZZ(60)
      GR=34.2
      RI=348.38
204  NC=9
      200 FORMAT (12).
      N1=1
      N2=NQ
C     READ IN ZZ ROW
205  DO 201 J=1,8
      N3=5*J-4
      N4=N3+4
201  READ(1,600,ERR=999)(ZZ(L),L=N3,N4)
      600 FORMAT (6X,5E14.7)
      601 FORMAT (2I2,2X,2E14.7,3E11.4,16,1X,3I2)
      N3=N3+5
      N4=N3+1
      READ(1,601,ERR=999) IREG,MONTH,(ZZ(L),L=N3,N4),Y7,GRT(6),
      1GRT(7),NPM,NGR,NL,NU
      GRT(5)=NGR
      GRT(5)=GRT(5)/1000.C
      PMM=NPM
      PMM=ALOG(PMM/100.0)
      DO 540 J=2,7
      IF(J-7) 1113,1111,1111
1111  YY(1)=Y7
      GO TO 1112
1113  DO 202 K=1,NQ
      N3=NC*(J-2)
      202 YY(K)=ZZ(N3+K)
C     COMPUTES 26 PTS IN J-TH COLUMN WITH JK(J) CCEFS YY(L) FOR GRT(J),D(J,K)
1112  DO 300 K=1,26
      XK=K-1
      IF(((J-7)*(J-6)).NE.0) GO TO 170
      IF(K-7) 170,920,921
200  IF(J.EQ.7) D(7,6)=SQRT(D(7,6))
201  D(J,K)=D(J,6)/EXP(GRT(J)*(XK-5.0))
      IF(J-6) 171,300,171
170  IF(XK.EQ.0.0) GO TO 111
      D(J,K)=0.0
      NX=NQ
      IF(J.EQ.6) NX=6
      IF(J.EQ.7) NX=1
      DO 80 L=1,NX
80  C(J,K)=D(J,K)+YY(L)*XK**(L-1)
      GO TO 652
111  C(J,1)=YY(1)
652  IF (J.EQ.3) GO TO 653
      IF(J.LT.5) GO TO 654
      C(J,K)=D(J,K)/EXP(GRT(J)*XK)
654  IF (J.EQ.6) GO TO 300
171  C(J,K)=D(J,K)**2
      GO TO 300
653  C(J,K)=1.0/D(J,K)
300  CONTINUE
      IF(J.NE.3) GO TO 540
699  DO 655 I=1,26
      D(1,I)=0.0
655  D(8,I)=0.0
      DO 656 K=1,26
      XK=K-1

```

658 DO 657 L=1,NX

XH=L

657 D(1,K)=D(1,K)+YY(L)* XK ** L/XH

C(1,K)=EXP(PMM-GR*D(1,K))

656 C(8,K)=D(1,K)*RI/D(3,K)

540 CONTINUE

422 C(7,6)=D(7,6)**2

C END COMPUTE

WRITE(3,9696)MONTH,D(1,1),D(1,1),IREG

9696 FORMAT(1H1,4X,34HFOUR-DIMENSIONAL ATMOSPHERIC MODEL//17X,7HMONTH
1=,13,14X,10HLATITUDE =,F8.2,3X,11HLONGITUDE =,F8.2,2H E,12X,6HREGI
2ON,13//17X,5HLEVEL,3X,8HPRESSURE,2X,9H VARIANCE,2X,8HTEMP (K),2X,8H
3VARIANCE,1X,10H WATER,10H VARIANCE,10H DENSITY,9H VARIANCE/
4/)

DO 744 K=1,26

N=K-1

744 WRITE(3,9697) N,(D(L,K),L=1,4),(D(M,K),M=6,8),D(5,K)

9697 FORMAT(16X,12,3H KM,2X,8F10.2)

999 RETURN

END

REFERENCES

1. Bastuscheck, C. P., "Ground Temperature and Thermal Infrared", Photogrammetric Engineering, October, 1970, pp. 1064-1072.
2. Anding, D., Kauth, R., and Turner, R., "Atmospheric Effects on Infrared Multispectral Sensing of Sea-Surface Temperature From Space", NASA CR-1858, July 1971.
3. Chang, D., Fowler, M., "Use of 4-D Atmospheric Models in the Simulation of Radiometric Measurements", NASA-CR-129007, July, 1973.
4. McNeill, W., Elliott, J., and Dixon, B., "Atmospheric Effects on Remote Sensing of Non-Uniform Temperature Sources," NASA CR-129004, May 22, 1973.
5. Sparrow, E. M. and Cess, R. D., Radiation Heat Transfer, Brooks/Cole Publishing Company, 1966.
6. Chandrasekhar, S., Radiative Transfer, Dover Publications, 1960.
7. Planck, M., The Theory of Heat Radiation, Dover Publications, New York, 1959.
8. Miller, B. P., Beck, G. A., and Barletta, J. M., "High Resolution Multispectral Camera System for ERTS A & B", J. Spacecraft, Volume 10, No. 10, October, 1973, pp. 638-646.
9. SKYLAB-A/EREP Users Handbook, NASA-S-72-831-V, April 1972.
10. Gates, D., "Spectral Distribution of Solar Radiation at the Earth's Surface," Science, Volume 151, No. 3710, February 4, 1966, pp. 523-529.
11. Davis, P., and Rabinowitz, P., Numerical Integration, Blaisdell Publishing Company, 1967.
12. Bulirsch, R., "Bemerkungen zur Romberg - Integration," Numerische Mathematic, 6, pp. 6-16, 1964.
13. Schönage, A., "Mehrdimensionale Romberg - Integration," Numerische Mathematic, 14, pp. 299-304, 1970.
14. Antes, H., "Über die vierdimensionale Romberg - Integration mit Schranken," Computing, 9, pp. 45-52, 1972.
15. Anders, E., "An Extension of Romberg Integration Procedures to N-Variables," JACM 13, 505-510, 1966.
16. Threlkeld, J. L., and Jordan, R. C., "Direct Solar Radiation Available on Clear Days," ASHACE Journal, Volume 64, 1958, pp. 45-68.

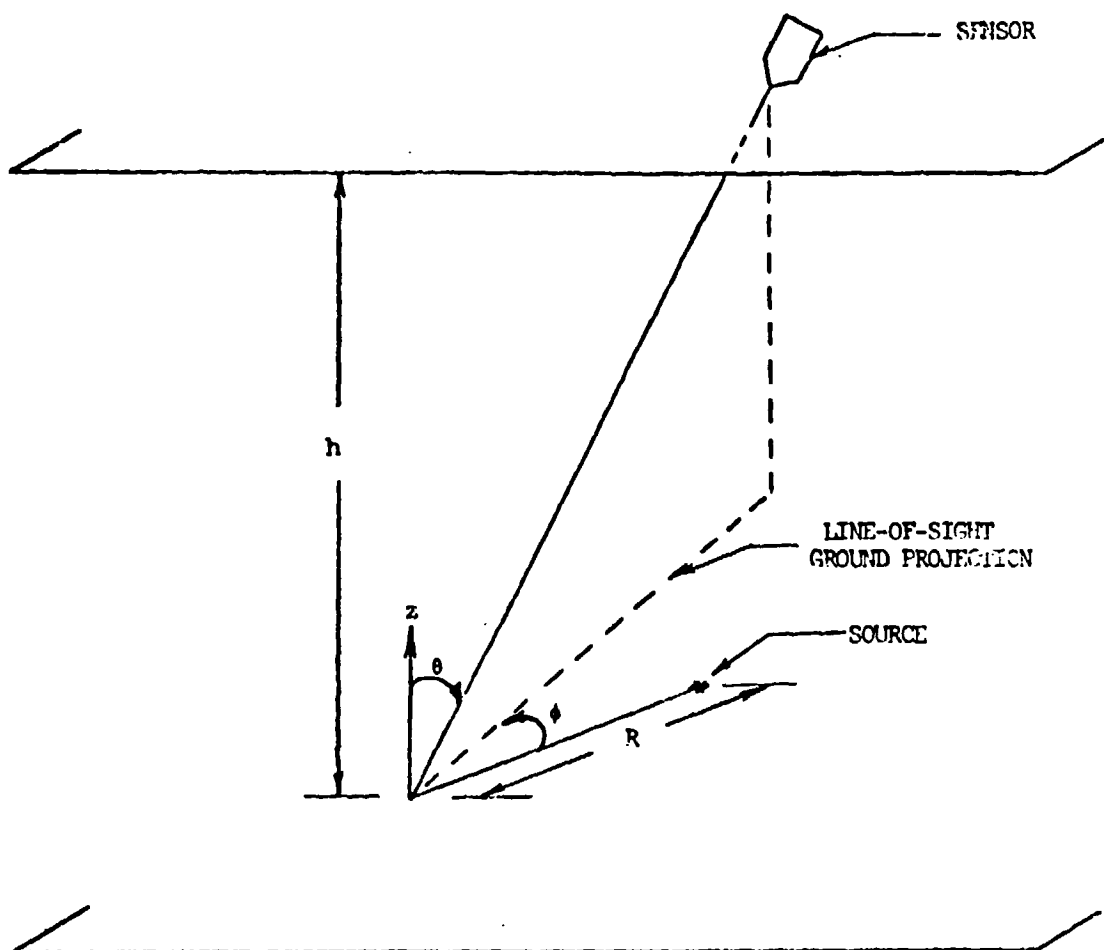


FIGURE 1

GEOMETRY OF SENSOR LINE-OF-SIGHT FOR
POINT SOURCE EMISSION WITH SCATTERING ATMOSPHERE

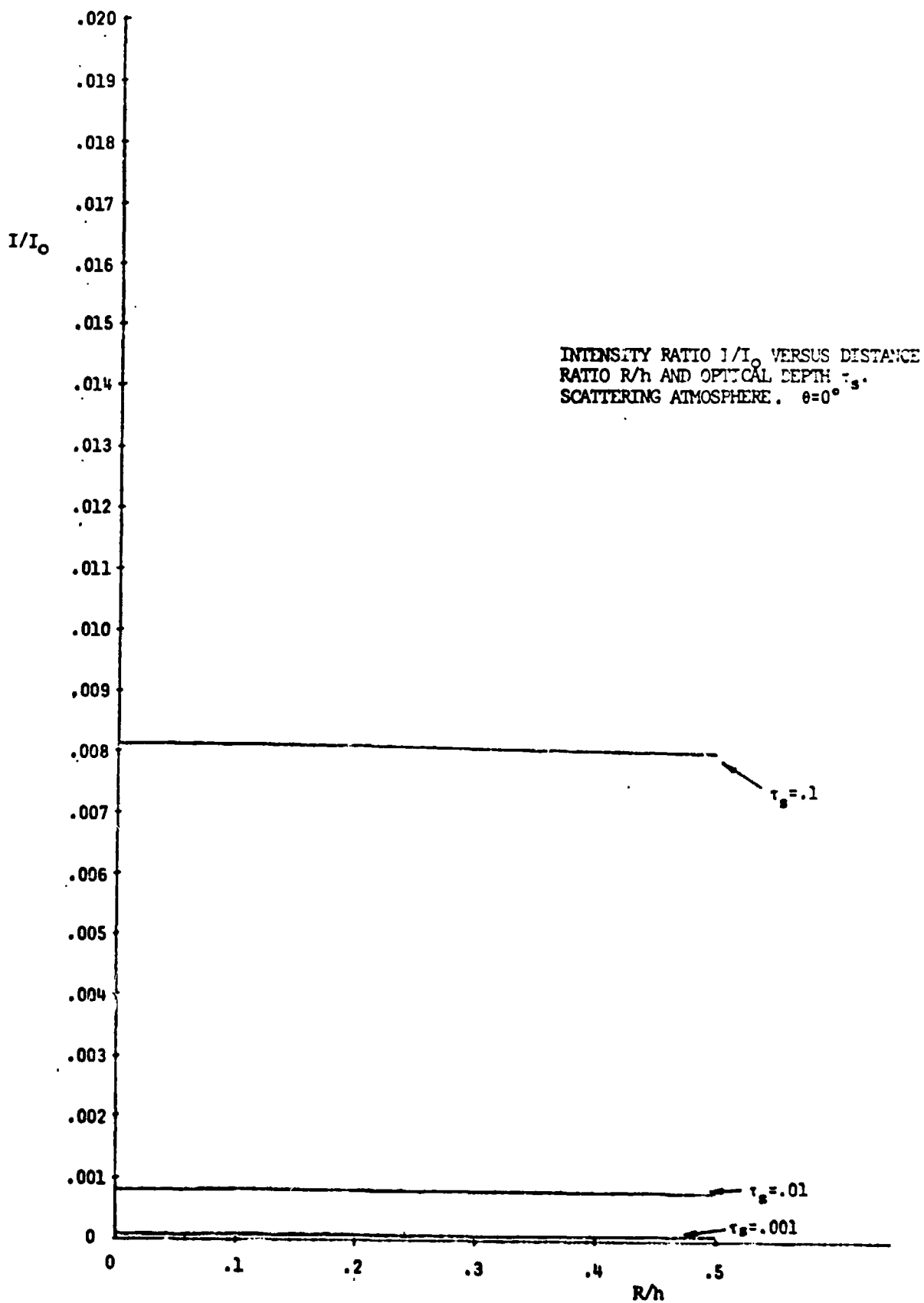


FIGURE 2

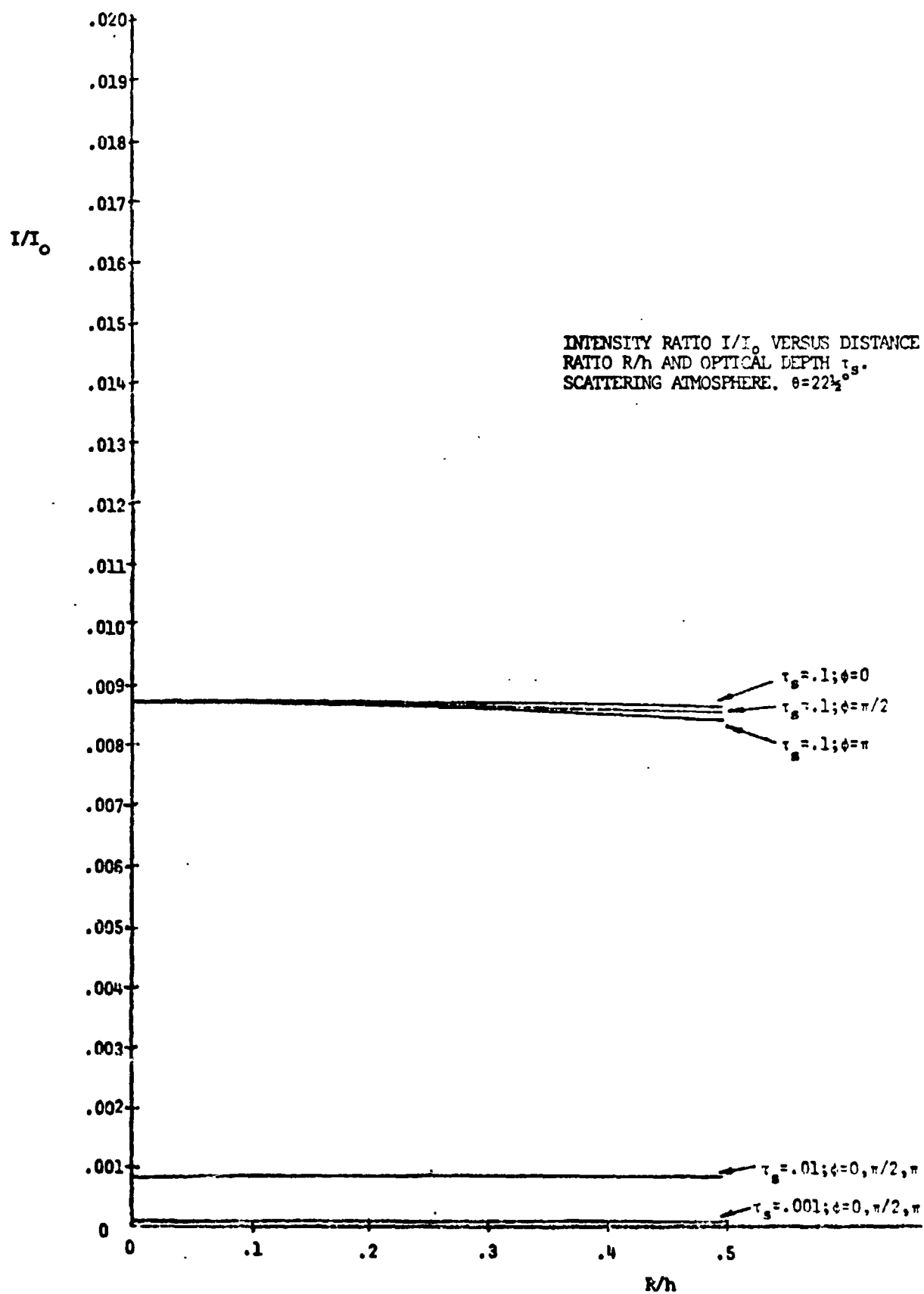


FIGURE 3

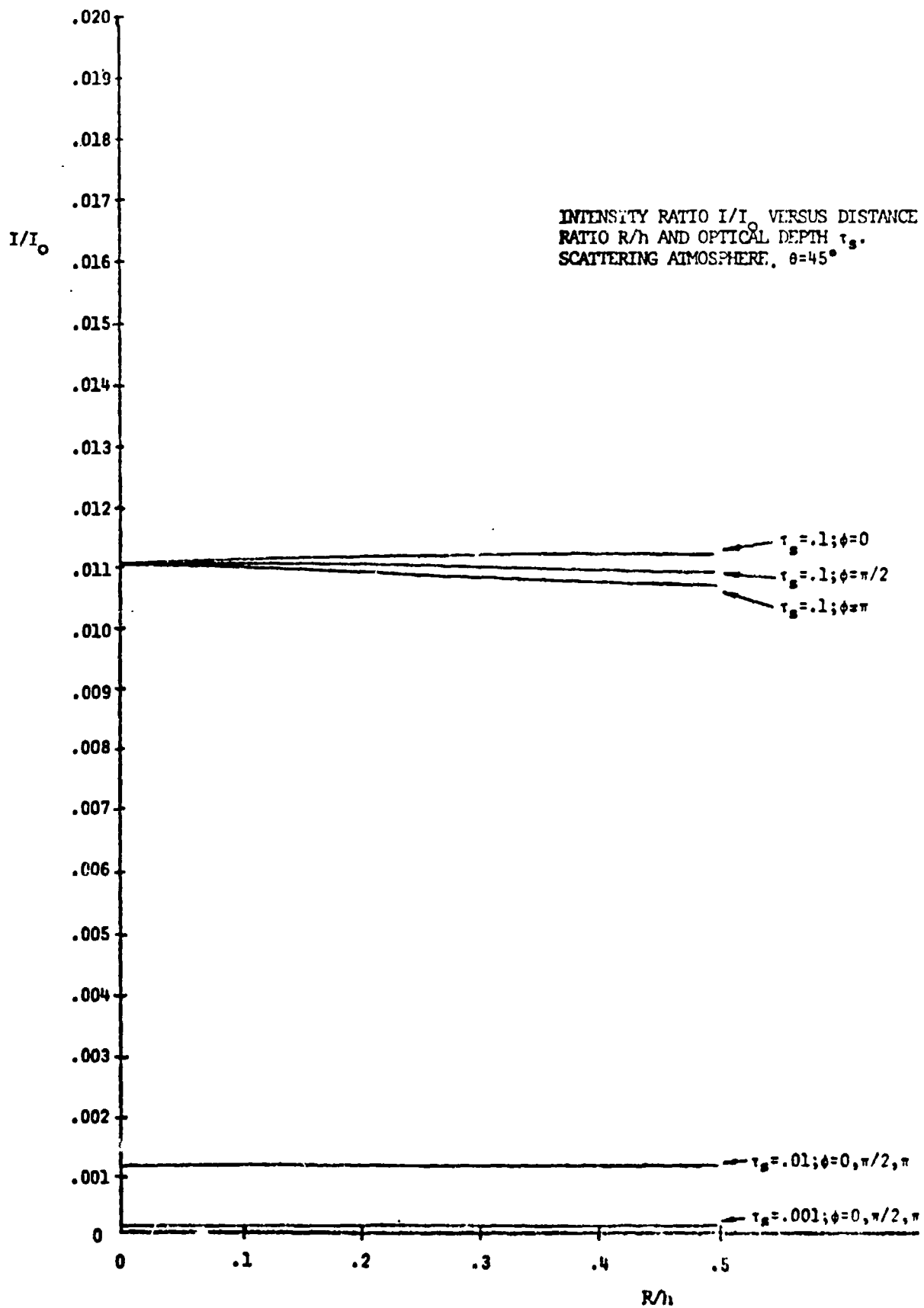


FIGURE 4

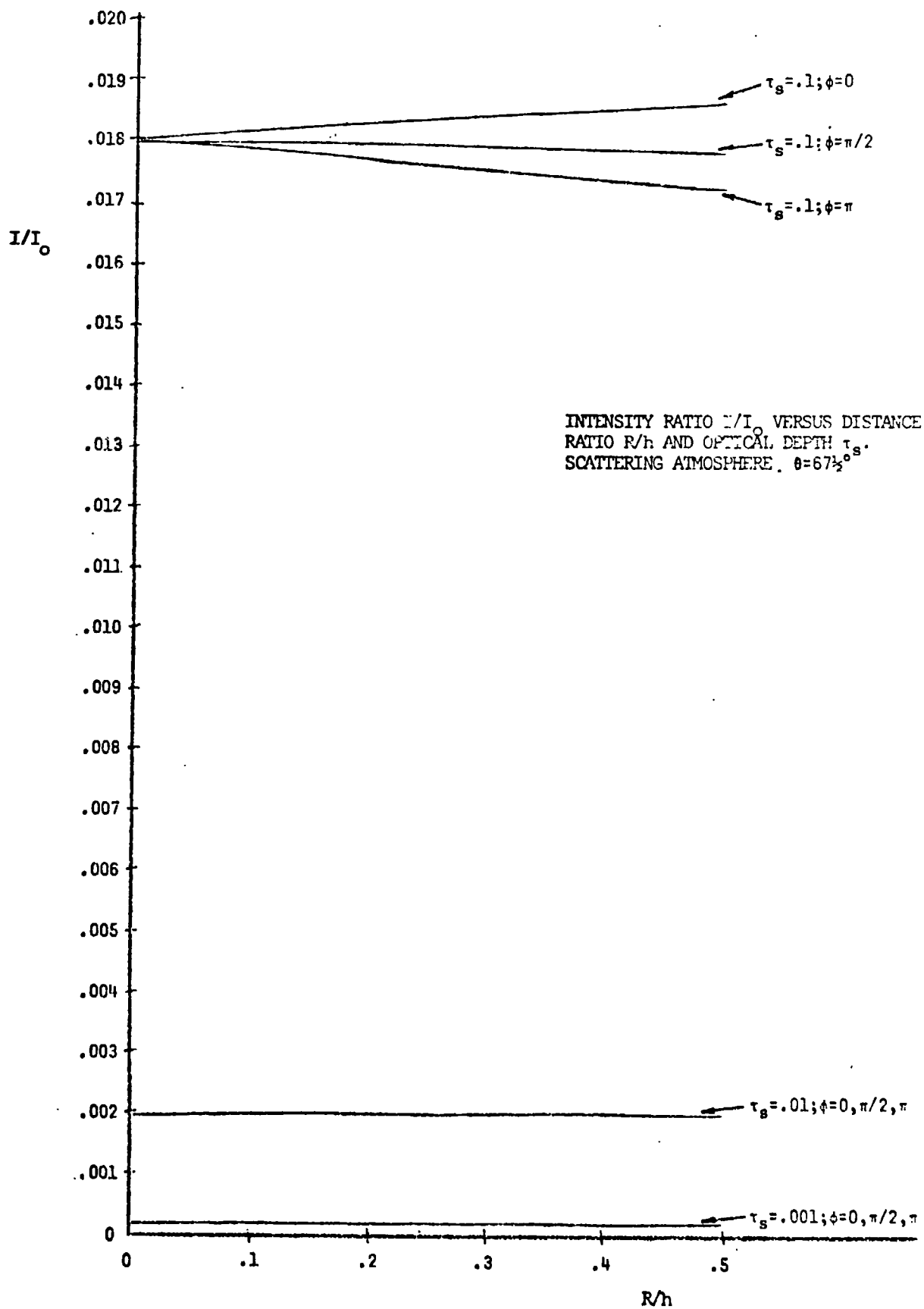


FIGURE 5

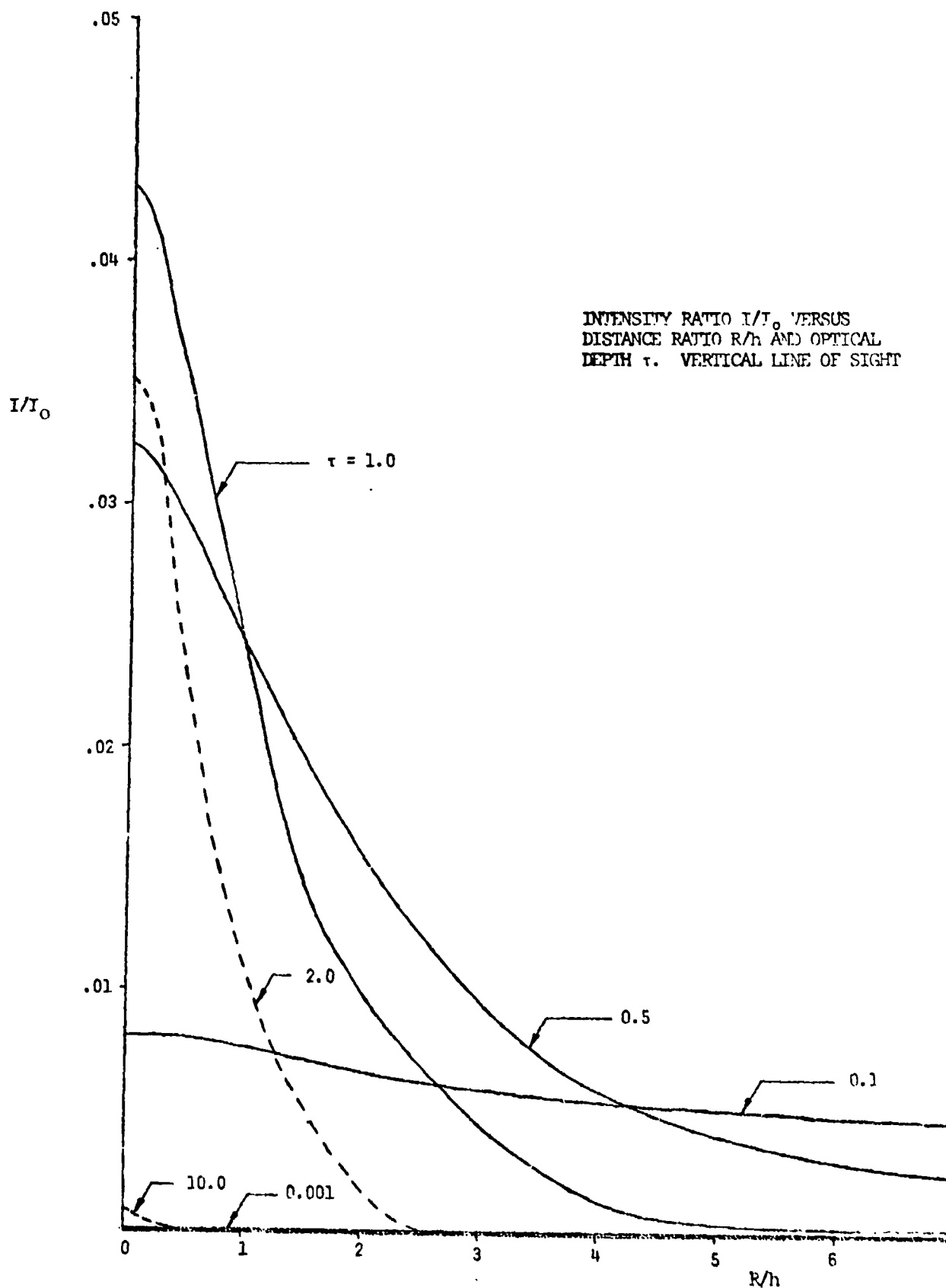


FIGURE 6

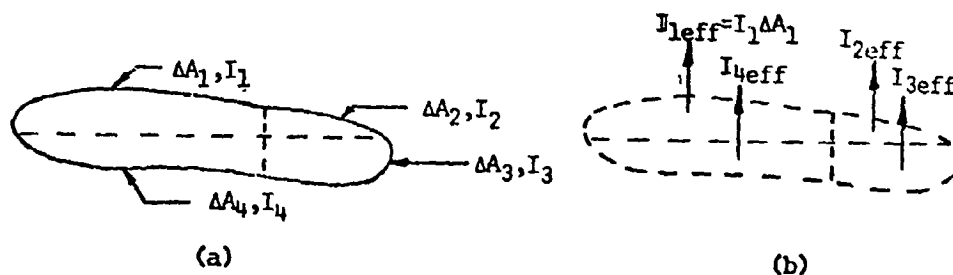


FIGURE 7

Establishment of Emission Point Sources in an Area of Non-Uniform Intensity

- (a) Emitting surface area A , having non-uniform intensity. $A = \sum \Delta A_i$
- (b) Replacement of emitting surface area by point sources. $I_{ieff} = I_i \Delta A_i$

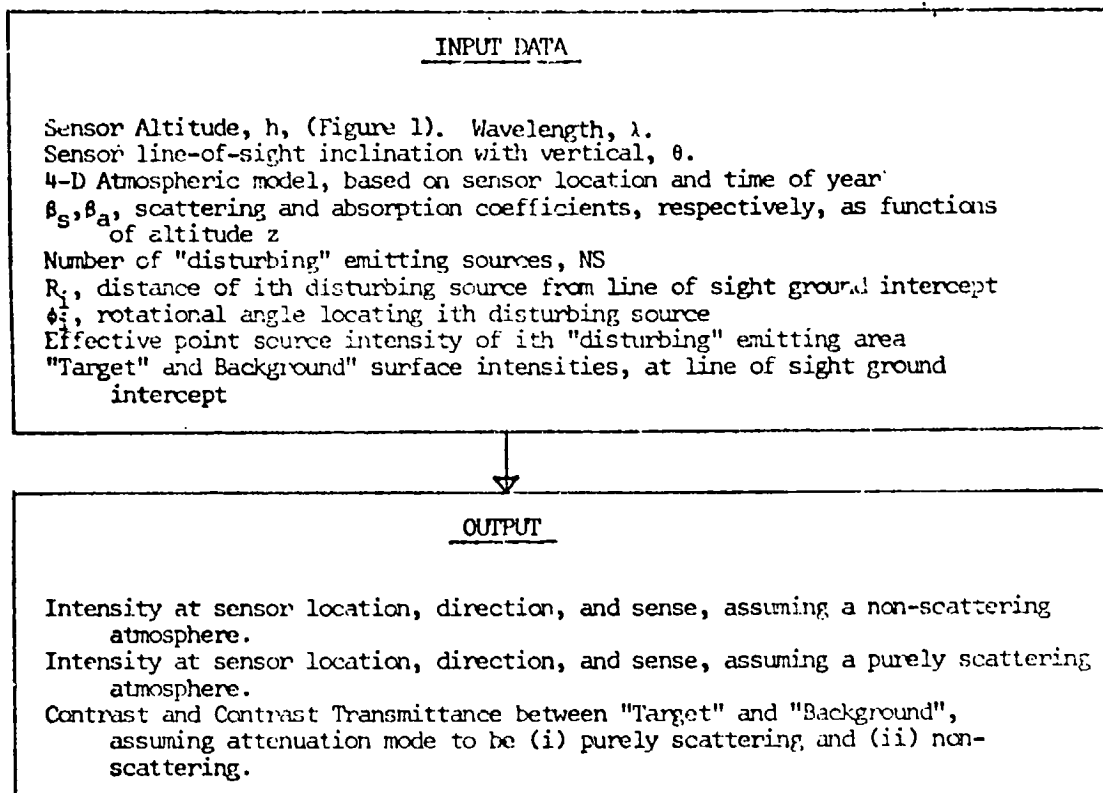


FIGURE 8
INPUT AND OUTPUT DATA FOR COMPUTER PROGRAM
LISTED IN APPENDIX II

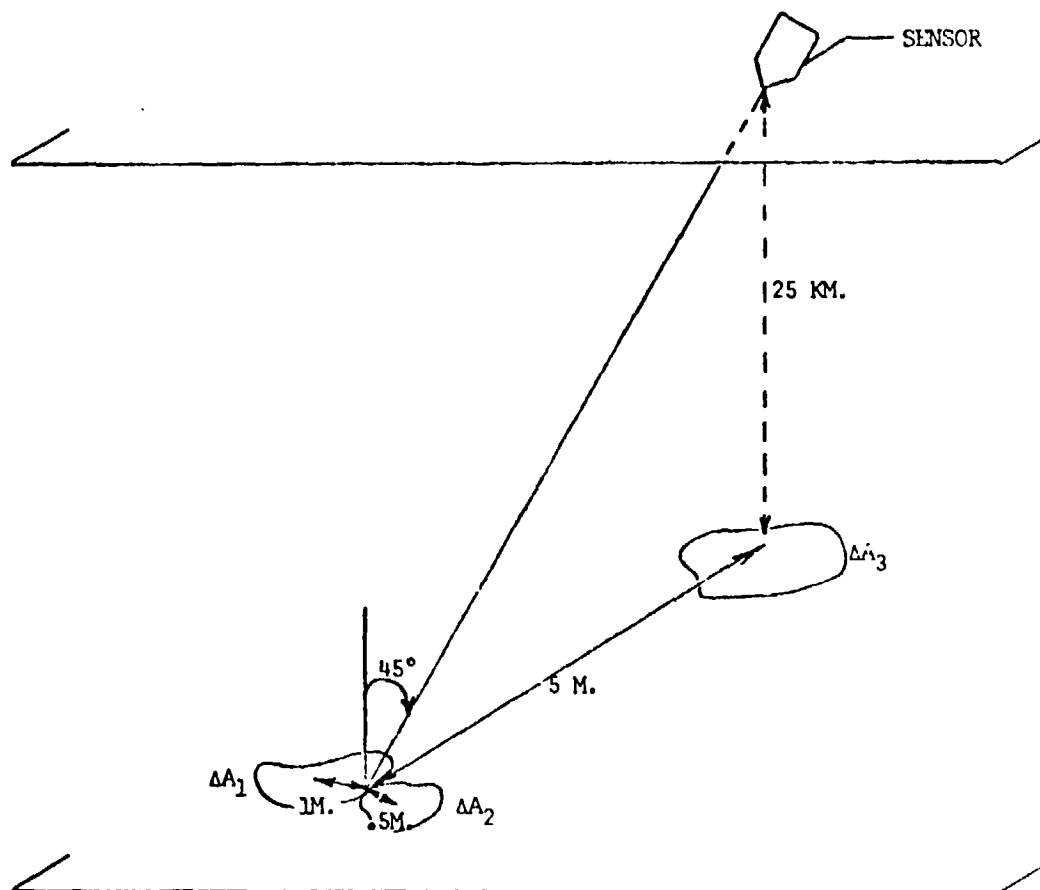


FIGURE 9

GEOMETRY OF EXAMPLE ILLUSTRATING
COMPUTATION OF CONTRAST TRANSMITTANCE